# On-chip experiment for chiral mode transfer without enclosing an exceptional point

Qingjie Liu,[1] Jibing Liu,[1] Dong Zhao,[2,*] and Bing Wang[3,†]

[1]*College of Physics and Electronic Science, Hubei Normal University, Huangshi 435002, China*

[2]*School of Electronics Information and Engineering, Hubei University of Science and Technology, Xianning 437100, China*

[3]*School of Physics and Wuhan National Laboratory for Optoelectronics, Huazhong University of Science and Technology, Wuhan 430074, China*

(Received 3 November 2020; revised 20 January 2021; accepted 15 February 2021; published 25 February 2021)

Adiabatically encircling an exceptional point (EP) in a two-dimensional parameter space usually leads to the flip of instantaneous eigenstates. However, encircling dynamically the EP will arouse chiral modes transfer. The obtained eigenstate is determined by the encircling direction. The effect is robust against the size of the encircling loop in the parameter space once the EP is enclosed in the loop. It has been reported theoretically that the effect can also be observed when the loop does not enclose EP but keeps it at a proper distance. Here we experimentally validate the theoretical prediction by designing and fabricating a silicon-on-insulator based subwavelength grating waveguides structure. The chiral modes transfer is achieved via motivating and detecting the even and odd modes around the telecommunication wavelength. The results provide a more robust way for studying the topological properties of the non-Hermitian system.

DOI: 10.1103/PhysRevA.103.023531

## I. INTRODUCTION

If an optical system contains open boundary or dissipation, the eigenvalues of the Hamiltonian are usually complex and many unique properties have been discovered [1–8]. A prominent example came from the degeneracy of the eigenvalues and eigenvectors. The degeneracy points are known as exceptional points (EPs) [9,10]. Numerous phenomena associated with EPs have been observed in waveguide and cavity arrangements, for example, loss induced transparency [11], unidirectional invisibility [12], sensor to perturbations [13], and single-mode laser [14]. Besides, adiabatically or dynamically encircling an EP has been also widely studied to investigate the topological property of non-Hermitian systems [15–18]. For adiabatic encircling, the instantaneous eigenstates will transfer to another while gaining a geometric phase. As the encircling becomes dynamic, the output eigenstate depends on the encircling direction, leading to chiral modes transfer [17–19].

The chiral modes transfer by encircling an EP has been theoretically studied and experimentally realized in metallic waveguides [20], optomechanical systems [21], ferromagnetic waveguides [22], and silicon-on-insulator (SOI) optical platforms [23–26]. The devices are designed to perform varying structure parameters which form a closed loop enclosing an EP. Actually, the effect still exists even without enclosing an EP in a dynamic circle, which is just required to be in the direct vicinity of EP [27,28]. It is because the nonadiabatic transition in the vicinity of EP remains strong even if the instantaneous eigenvalues do not intersect along the parameter loop. The condition expands the boundary of encircling loop desired for chiral transfer processes.

In this work, we implement an experiment to demonstrate the chiral modes transfer without encircling the EP. The structure is designed and fabricated based on silicon-on-insulator (SOI) subwavelength grating (SWG) waveguides, which enable precise control of structure parameters. By adjusting the parameters, the coupling strength and resonance detuning of modes in individual waveguides can be flexibly modulated, and form a closed loop without enclosing the EP. We numerically calculate mode transfer efficiency influenced by the distance between the loop and EP. Meanwhile, two eigenmodes are separately motivated and detected in both ends of the waveguides, providing experimental validation of theory. The results show that chiral modes transfer is observed. Our research may find practical applications in on-chip optical devices such as mode converters, and the SWGs waveguide offers a platform for the study of non-Hermitian dynamics.

## II. THEORETICAL MODEL

We start from considering an optical waveguide structure consisting of two SWG waveguides, as shown in Fig. 1(a). The amplitudes of the transverse-electric-like modes in the individual waveguides abide by the Schrödinger-type equation

$$i\frac{d}{dz}\begin{pmatrix}A_1\\A_2\end{pmatrix}=H\begin{pmatrix}A_1\\A_2\end{pmatrix}=\begin{pmatrix}\alpha+\Delta\alpha & C\\ C & \alpha+i\gamma\end{pmatrix}\begin{pmatrix}A_1\\A_2\end{pmatrix}, \quad (1)$$

where $A_{1,2}$ stand for the mode amplitudes in the individual waveguides. $\alpha$ is the propagation constant, and $\Delta\alpha$ represents the amount of detuning. $\gamma$ is the propagation loss, and the coupling strength is denoted by $C$. The model is slightly different than [27] which introduced both loss and gain components in the system. The difference takes no effect on the theoretical research.

*zhaodong@hbust.edu.cn

†wangbing@hust.edu.cn

 

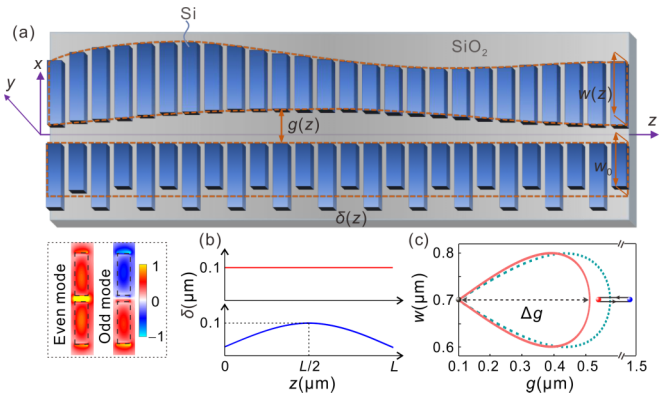


FIG. 1. (a) Schematic of the two SWG waveguides. Inset in the dashed box depicts profiles of even and odd modes at both ends of the waveguides. (b) Uniform and nonuniform distributions of fluctuation amplitude $\delta$ along the propagation direction. (c) Trajectory of parameter loops enclosing (dotted curve) and not enclosing (solid curve) the EP (red sphere). The terminal point of the loops is indicated by the gray sphere. The incident wavelength is chosen as $\lambda = 1550$ nm.

By solving the Hamiltonian $H$, we obtain the eigenvalues $S_\pm = (2\alpha + \Delta\alpha + i\gamma)/2 \pm [(\Delta\alpha - i\gamma)^2 + 4C^2]^{1/2}/2$ and the eigenvectors $[1, (S_\pm - \alpha - \Delta\alpha)/C]^{\mathrm{T}}$. Once the parameters satisfy $\Delta\alpha = 0$ and $C = \gamma/2$, both the eigenvalues and eigenvectors of the Hamiltonian coalesce, leading to the appearance of an exceptional point (EP). The SWGs are fabricated based on the SOI technique by using a 220-nm-thick Si layer with a 3-$\mu$m-thick buried $SiO_2$ substrate. There is only a fundamental TE mode in each SWG waveguide. The elements in Hamiltonian $H$ can be tailored by changing the geometric parameters of the SWGs. Differing from Dirac points, the degeneracy points in the Hermitian system, EPs exist in a system with gain or loss. Here we introduce scattering loss to the system by applying periodically fluctuated width to one waveguide. The average width of the lossy waveguide is $w_0 = 0.7\,\mu$m and the fluctuation amplitude of the SWG strips is denoted by $\delta(z)$. Thus the propagation loss $\gamma$ is parametrized as $\gamma(\delta)$, and $\gamma$ increases with the increase of $\delta$. The other waveguide is lossless and has varying width $w(z)$. $g(z)$ denotes the gap distance between the lossy and lossless waveguides. The period and filling factor of the SWGs are separately fixed at $\Lambda = 0.3\,\mu$m and $f = 0.565$. The operating photon energy around $\lambda = 1550$ nm is far below the band gap of the SWGs such that Bragg scattering is avoided [26].

In the proposed waveguide system, we construct a two-dimensional parameter space by width $w$ and gap distance $g$, which determine the detuning $\Delta\alpha$ and coupling strength $C$ in Hamiltonian $H$, respectively. The width and gap vary as

$$g(z) = g_0 + \Delta g \sin(\pi z/L),$$
$$w(z) = w_0 \pm \Delta w \sin(2\pi z/L), \qquad (2)$$

where $w_0 = 0.7$, $\Delta w = 0.1$, and $g_0 = 0.1\,\mu$m. The sign $+$ $(-)$ represents clockwise (anticlockwise) encircling directions. As the propagation distance increases from $z = 0$ to $L$, the two parameters produce a closed loop in the $(g, w)$ plane with its size tuned by $\Delta g$. The terminal point of the loop locates at $w_0 = 0.7$ and $g_0 = 0.1\,\mu$m where $z = 0$ or $L$, corresponding to the ends of the waveguides. The profiles of even and odd modes in the terminal point are illustrated in the dashed box. According to the degeneracy condition, an EP in the parameter space surely locates at $w_{\mathrm{EP}} = w_0 = 0.7\,\mu$m and $g_{\mathrm{EP}} = g_{\mathrm{EP}}(\delta)$. In the following, we first consider uniform distribution of $\delta$ along the propagation direction. We set $\delta(z) = 0.1\,\mu$m, as shown by the upper line in Fig. 1(b). Through numerical simulation [26,29,30], a fixed EP is confirmed in the position of $g_{\mathrm{EP}} = 0.52\,\mu$m, indicated by the red sphere in Fig. 1(c). The solid loop without enclosing the EP and dotted loop enclosing the EP are plotted according to Eq. (2), in which $\Delta g < 0.42\,\mu$m and $\Delta g > 0.42\,\mu$m, respectively. Then we consider a nonuniform distribution of $\delta$, which is set to be variable following a Gauss distribution $\delta(z) = \delta_0 \exp[-(z-L/2)^2\rho^2/L^2]$ with $\delta_0 = 0.1\,\mu$m and $\rho = 3.5$. The lower curve in Fig. 1(b) plots the nonuniform distribution of $\delta$. Loss decreases from the middle to both ends of the waveguide gradually, leading to moving EPs in the system [26]. As shown in Fig. 1(c), the EP is initially located in the position implied by the blue sphere. With increasing the propagation distance, the EP moves to the red sphere as $z = L/2$ and finally returns to the original blue sphere. Our previous work has shown that topological mode transfer still happens even if the moving EP is enclosed transiently by the encircling loop [26]. Specifically, the EP in $z = L/2$ should be enclosed by the loop. Otherwise, the loop does not encircle the EP and instantaneous mode transfer will not occur. Compared to the fixed EP ($\rho = 0$), utilizing moving EPs ($\rho = 3.5$) can significantly reduce the loss and length of the structure.

## III. RESULTS AND DISCUSSION

### A. Modes transfer efficiency influenced by gap distance

The evolution of modes in the designed waveguide structure is simulated by the finite-difference time-domain (FDTD) method. The length of the waveguides is set to $L = 69\,\mu$m which is long enough to ensure adiabatic parameter evolution [23–26]. The even and odd modes can be separately motivated in one end and detected in the other end of the waveguides. We employ $T_{ij}$ ($T'_{ij}$) as transmittance from mode $i$ into mode $j$ for the clockwise (anticlockwise) encircling direction, where $i, j = 1$ or 2 represents the even or odd mode. Figures 2(a)–2(d) plot the simulated transmittance $T_{ij}$ as a function of $\Delta g$. The vertical dashed line indicates the position where the loop exactly goes through the EP in $z = L/2$, that is $\Delta g = g_{\mathrm{EP}} - g_0$. As for $T'_{ij}$, it can be obtained from the reciprocity relation of $T'_{ij} = T_{ji}$ in the system. Comparing the case of $\rho = 0$ with $\rho = 3.5$, we find the former has significantly lower transmittances because that mode evolution suffers less loss in the waveguide structure with nonuniform fluctuation amplitude $\delta$.

The transfer efficiency can be characterized by the power ratio of output even mode. We denote $\eta_e$ ($\eta'_e$) as the even-to-total power ratio at the output for clockwise (anticlockwise) encircling. As the even mode is incident, it is defined as $\eta_e = T_{11}/(T_{11} + T_{12})$ for clockwise encircling and $\eta'_e = T'_{11}/(T'_{11} + T'_{12})$ for anticlockwise encircling. As the odd mode is incident, it is defined as $\eta_e = T_{21}/(T_{21} + T_{22})$ for clockwise encircling and $\eta'_e = T'_{21}/(T'_{21} + T'_{22})$ for anticlockwise encircling. The simulated transfer efficiency as a

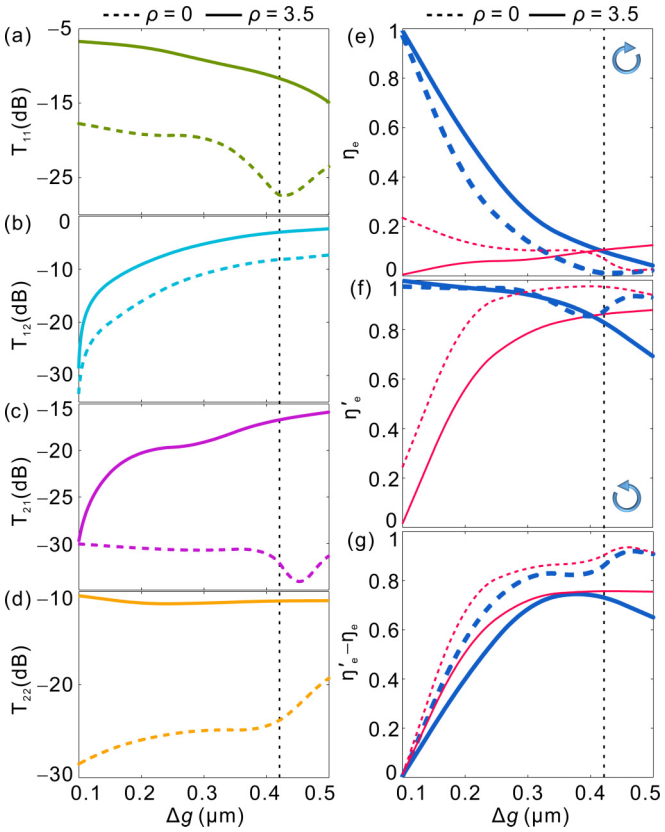


FIG. 2. (a)–(d) Transmittance as a function of gap distance $\Delta g$. (e), (f) Transfer efficiency as a function of $\Delta g$. The encircling direction is clockwise in (e) and anticlockwise in (f). (g) Difference of transfer efficiency in the two directions. The thick and thin curves denote incidence of even and odd modes, respectively. The solid and dashed curves represent uniform and nonuniform loss distribution, respectively. The vertical dashed lines indicate that the loop exactly goes through the EP, $\Delta g = g_{\mathrm{EP}} - g_0 = 0.42\,\mu$m.

function of $\Delta g$ is plotted in Figs. 2(e) and 2(f). The thick and thin curves depict incidence of even and odd modes, respectively. For uniform loss distribution ($\rho = 0$), the transfer efficiency as a function of $\Delta g$ is plotted by the dashed curves. As the loop is far away from the EP, $\Delta g \ll g_{\mathrm{EP}} - g_0$, the transfer efficiencies are fairly low for odd mode incidence and approach 100% for even mode incidence. It means that the output is still the incident mode despite the encircling directions. There is almost no mode transfer to occur. With the increase of $\Delta g$, the encircling loop gets closer to the EP. For even mode incidence, the value of $\eta_e$ decreases remarkably in the clockwise direction and $\eta_e'$ changes slightly in the anticlockwise direction. For odd mode incidence, the value of $\eta_e$ changes slightly in the clockwise direction and $\eta_e'$ increases remarkably in the anticlockwise direction. The difference of transfer efficiency in the two directions exceeds $\eta_e' - \eta_e = 0.8$ as $\Delta g > 0.3\,\mu$m [Fig. 2(g)], signifying highly asymmetric mode transfer. The output mode becomes the even one in the anticlockwise direction and keeps the odd one in the clockwise direction. Finally, the transfer efficiency remains stable as $\Delta g$ is further increased to beyond $g_{\mathrm{EP}} - g_0$. The results show that asymmetric mode transfer still happens even if the encircling loop does not enclose the EP but gets close to

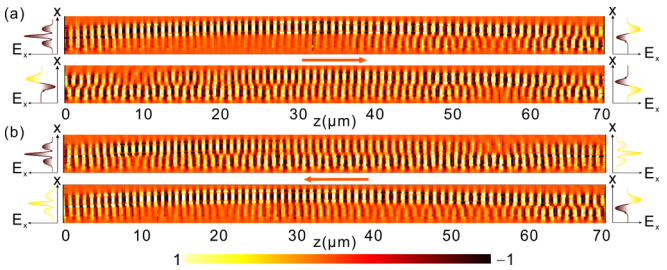


FIG. 3. Numerically simulated $E_x$ field distributions in the SWG waveguides. The incident mode is injected from (a) the left side and (b) the right side. The insets at both ends of the structure show the computed field profile along the $x$ direction at the input and output ports. Here we set $\rho = 3.5$ and $\Delta g = 0.35\,\mu$m.

it. The main reason is the existence of strong nonadiabatic transitions in the vicinity of EPs.

For nonuniform loss distribution ($\rho = 3.5$), the transfer efficiency as a function of $\Delta g$ is plotted by the solid curves, which share a similar trend as $\rho = 0$. The main difference is the degree of asymmetry ($\eta_e - \eta_e'$) in the two encircling directions, which is lower for $\rho = 3.5$. Even so, the difference of transfer efficiency in the two directions still exceeds 0.7 as $\Delta g > 0.3\,\mu$m [Fig. 2(g)], implying asymmetric mode transfer. To sum up, asymmetric mode transfer occurs even if the dynamic encircling loop does not enclose an EP, and modes suffer less loss when adopting moving EPs or nonuniform loss distribution.

The electric field distributions in the waveguides are given in Fig. 3, which is obtained by FDTD simulations. The fields are normalized in each propagation direction to evidently reveal the mode transfer process. When the even and odd modes are injected from the left, corresponding to clockwise encircling, we always obtain the odd mode at the output, as observed from the asymmetric distribution of the output electric field ($E_x$) shown in Fig. 3(a). Alternatively, when the even and odd modes are injected from the right, corresponding to anticlockwise encircling, the even mode with a symmetric field distribution is observed at the left output, as shown in Fig. 3(b).

### B. Measured and simulated spectra of transmittance

To validate the above results in experiment, we fabricate the structure by using electron-beam lithography with reactive ion etching on a commercial SOI platform. The amplitude of the gap distance and the loss distribution factor are set to $\Delta g = 0.35\,\mu$m and $\rho = 3.5$, respectively. Figure 4(a) illustrates the scanning electron microscope images of part of SWG waveguides and a mode converter [31–34]. On the chip, two converters are connected to both ends of the waveguides by gradually changing the waveguide geometry from a strip to a SWG. Besides, the structure contains an ancillary circuit composed of mode multiplexer (demultiplexer) and input (output) grating coupler [26]. The former is cascaded to realize mode-division multiplexing of the two lowest order TE modes, and the latter couples light in each output channel into the single-mode fiber or vice versa. The experimental setup used for mode motivation and measurement is schematically

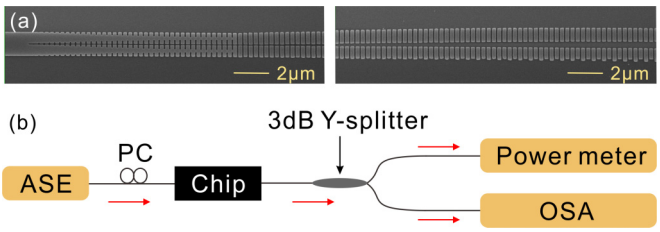


FIG. 4. (a) Scanning electron microscopy images of one converter and part of the SWG waveguides. (b) Schematic of the experimental setups. The structure on chip contains the SWG waveguides and the ancillary optical circuits.

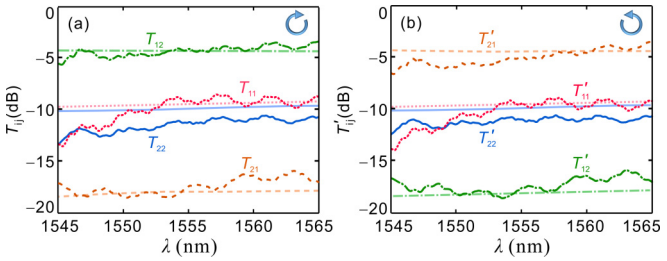


FIG. 5. Experimentally measured (dark color) and FDTD simulated (light color) spectral responses for clockwise (a) and anticlockwise (b) encircling direction. We set $\Delta g = 0.35\,\mu$m, $\rho = 3.5$, and $L = 69\,\mu$m.

illustrated in Fig. 4(b). A wideband amplified spontaneous emission (ASE) light source is used in our measurement. The continuous-wave ASE light is passed through a polarization controller to tune the polarization to TE. Then the light is coupled into and out of the chip vertically with single-mode fibers by the grating couplers. After the output fiber, a commercial 3-dB Y splitter is connected to split the output light into two paths. One is linked to the optical power meter for monitoring and tuning the alignment between the single-mode fibers and the grating couplers. The other is connected to the optical spectrum analyzer to measure the transmittance spectra for every mode.

The measured transmittances are plotted by the dark colored curves in Fig. 5 where the light colored curves depict FDTD-simulated spectra. The simulated transmittances at $\lambda = 1550\,$nm are identical to those in Figs. 2(a)–2(d) as $\Delta g = 0.35\,\mu$m and $\rho = 3.5$. The experimental results agree well with the simulation over a wavelength range of 1545–1565 nm. The range can be broadened by designing the ancillary optical circuits operating in a wider bandwidth centered at 1550 nm. For the oscillation in the measured spectra, it is caused by reflection from connections of the SWG waveguides and converters [26]. As the even mode is incident forwardly (clockwise encircling), we have $T_{12}$–$T_{11} \sim 6\,$dB meaning the output is mainly the odd mode. Most of the even mode transfers to the odd. As the odd mode is incident forwardly, one sees that $T_{22}$–$T_{21} \sim 7\,$dB, which means that the output is still dominated by the odd mode. On the other hand, as the mode is incident backwardly (anticlockwise encircling), the transmittances satisfy $T'_{11} > T'_{12}$ and $T'_{21} > T'_{22}$ for the incidence of even and odd modes, respectively. The even mode always dominates at the output. In consequence, the output mode is determined by the encircling direction despite the input mode.

## IV. CONCLUSIONS

In conclusion, we have designed and fabricated a waveguide structure to realize the chiral mode transfer by dynamically changing two parameters forming a closed loop. With the increase of gap variation amplitude, the loop becomes larger and gets closer to the EP. As the loop does not enclose the EP, the transfer efficiency can still remain at a high level as long as the loop is in the vicinity of the EP. Experimentally, the even and odd modes in both ends of the waveguides are separately motivated and detected by adopting additional circuits and setups. The measured spectra of transmittance coincide with those obtained by numerical simulation. The waveguide's own compact size facilitates integration into other on-chip structures. The results broaden the condition needed for chiral transfer, providing a more robust way to study the topological properties of the non-Hermitian system.

## ACKNOWLEDGMENT

The work was supported by the National Natural Science Foundation of China (Grants No. 11674117, No. 11974124, No. 12021004, and No. 12004188).

[1] C. E. Rüter, K. G. Makris, R. El-Ganainy, D. N. Christodoulides, M. Segev, and D. Kip, Nat. Phys. **6**, 192 (2010).
[2] A. Regensburger, C. Bersch, M.-A. Miri, G. Onishchukov, D. N. Christodoulides, and U. Peschel, Nature (London) **488**, 167 (2012).
[3] C. M. Bender and S. Boettcher, Phys. Rev. Lett. **80**, 5243 (1998).
[4] M. V. Berry, Czech. J. Phys. **54**, 1039 (2004).
[5] I. Rotter, J. Phys. A **42**, 153001 (2009).
[6] B. Zhen, C. W. Hsu, Y. Igarashi, L. Lu, I. Kaminer, A. Pick, S. Chua, J. D. Joannopoulos, and M. Soljačić, Nature (London) **525**, 354 (2015).
[7] X. Zhang, V. A. Vysloukh, Y. V. Kartashov, X. Chen, F. Ye, and M. R. Belić, Opt. Lett. **42**, 2972 (2017).
[8] A. A. Sukhorukov, Z. Xu, and Y. S. Kivshar, Phys. Rev. A **82**, 043818 (2010).
[9] B. Peng, Ś. K. Ozdemir, S. Rotter, H. Yilmaz, M. Liertzer, F. Monifi, C. M. Bender, F. Nori, and L. Yang, Science **346**, 328 (2014).
[10] B. Dietz, H. L. Harney, O. N. Kirillov, M. Miski-Oglu, A. Richter, and F. Schäfer, Phys. Rev. Lett. **106**, 150403 (2011).
[11] A. Guo, G. J. Salamo, D. Duchesne, R. Morandotti, M. Volatier-Ravat, V. Aimez, G. A. Siviloglou, and D. N. Christodoulides, Phys. Rev. Lett. **103**, 093902 (2009).

[12] Q. Liu, B. Wang, S. Ke, H. Long, K. Wang, and P. Lu, Opt. Express **25**, 7203 (2017).
[13] H. Hodaei, A. U. Hassan, S. Wittek, H. Garcia-Gracia, R. El-Ganainy, D. N. Christodoulides, and M. Khajavikhan, Nature (London) **548**, 187 (2017).
[14] L. Feng, Z. J. Wong, R.-M. Ma, Y. Wang, and X. Zhang, Science **346**, 972 (2014).
[15] T. Gao, E. Estrecho, K. Y. Bliokh, T. C. H. Liew, M. D. Fraser, S. Brodbeck, M. Kamp, C. Schneider, S. Höfling, Y. Yamamoto, F. Nori, Y. S. Kivshar, A. G. Truscott, R. G. Dall, and E. A. Ostrovskaya, Nature (London) **526**, 554 (2015).
[16] K. Ding, G. Ma, M. Xiao, Z. Q. Zhang, and C. T. Chan, Phys. Rev. X **6**, 021007 (2016).
[17] C. Dembowski, H. D. Gräf, H. L. Harney, A. Heine, W. D. Heiss, H. Rehfeld, and A. Richter, Phys. Rev. Lett. **86**, 787 (2001).
[18] C. Dembowski, B. Dietz, H.-D. Gräf, H. L. Harney, A. Heine, W. D. Heiss, and A. Richter, Phys. Rev. E **69**, 056216 (2004).
[19] A. U. Hassan, B. Zhen, M. Soljačić, M. Khajavikhan, and D. N. Christodoulides, Phys. Rev. Lett. **118**, 093002 (2017).
[20] J. Doppler, A. A Mailybaev, P. Rabl, N. Moiseyev, and S. Rotter, Nature (London) **537**, 76 (2016).
[21] H. Xu, D. Mason, L. Jiang, and J. G. E. Harris, Nature (London) **537**, 80 (2016).
[22] X. L. Zhang, S. Wang, B. Hou, and C. T. Chan, Phys. Rev. X **8**, 021066 (2018).
[23] J. W. Yoon, Y. Choi, C. Hahn, G. Kim, S. H. Song, K.-Y. Yang, J. Y. Lee, Y. Kim, C. S. Lee, J. K. Shin, H.-S. Lee, and P. Berini, Nature (London) **562**, 86 (2018).
[24] S. N. Ghosh and Y. D. Chong, Sci. Rep. **6**, 19837 (2016).
[25] Y. Choi, C. Hahn, J. W. Yoon, S. H. Song, and P. Berini, Nat. Commun. **8**, 14154 (2017).
[26] Q. Liu, S. Li, B. Wang, S. Ke, C. Qin, K. Wang, W. Liu, D. Gao, P. Berini, and P. Lu, Phys. Rev. Lett. **124**, 153903 (2020).
[27] A. U. Hassan, G. L. Galmiche, G. Harari, P. LiKamWa, M. Khajavikhan, M. Segev, and D. N. Christodoulides, Phys. Rev. A **96**, 052129 (2017).
[28] A. U. Hassan, G. L. Galmiche, G. Harari, P. LiKamWa, M. Khajavikhan, M. Segev, and D. N. Christodoulides, Phys. Rev. A **96**, 069908(E) (2017).
[29] C. Fietz, Y. Urzhumov, and G. Shvets, Opt. Express **19**, 19027 (2011).
[30] G. Parisi, P. Zilio, and F. Romanato, Opt. Express **20**, 16690 (2012).
[31] S. Li, Y. Zhou, J. Dong, X. Zhang, E. Cassan, J. Hou, C. Yang, S. Chen, D. Gao, and H. Chen, Optica **5**, 1549 (2018).
[32] X. Chen, C. Li, C. K. Y. Fung, S. M. G. Lo, and H. K. Tsang, IEEE Photon. Technol. Lett. **22**, 1156 (2010).
[33] Y. Ding, J. Xu, F. Da Ros, B. Huang, H. Ou, and C. Peucheret, Opt. Express **21**, 10376 (2013).
[34] D. Dai and J. E. Bowers, Nanophotonics **3**, 283 (2014).